Hindawi
International Journal of Antennas and Propagation
Volume 2020, Article ID 8833839, 14 pages
https://doi.org/10.1155/2020/8833839

Research Article

Novel Low-Cost Integrated Multiband Antenna Design Customized for Smartwatch Applications with SAR Evaluation

Brahim Fady,[1] **Abdelwahed Tribak**,[1] **Jaouad Terhzaz**,[2] **and Fatima Riouch**[1]

[1]*Department of Microwave and Communication Antenna Subsystems, INPT, Rabat, Morocco*
[2]*Department of Physics, CRMEF Casablanca-Settat, Casablanca, Morocco*

Correspondence should be addressed to Brahim Fady; brahim.fady@gmail.com

Received 17 September 2020; Revised 16 November 2020; Accepted 4 December 2020; Published 15 December 2020

Academic Editor: Giuseppe Torrisi

This paper presents a novel low-cost integrated multiband antenna design customized for smartwatch applications and wearable devices. The design consists in using a broadband planar patch antenna with circular microstrip lines and a miniaturized feeding-point with a structure of $30 \times 30 \times 1.6\ mm^3$, and it is easy to deploy inside the smartwatch and cost-effective for the wearable device industry. The parametric study and final dimensions of the design and the measured results of the reflection and radiation pattern are discussed. The antenna with maximum gain up to 6.6 dBi and S_{11} up to −22 dB exhibits excellent performance for all the frequencies required in wearable systems such as 1.9 GHz, 2.3 GHz, 2.4 GHz, 2.6 GHz, 5.2 GHz, and 5.8 GHz. We drew a comparison between similar research and this work in terms of antenna performance. Furthermore, we investigate the specific absorption rate (SAR) performance of the antenna for the smartwatch application, using both human hand wrist multilayer and SAM head mouth models. The SAR results in different positions for all the frequencies are compared to the Federal Communication Commission (FCC) standards.

1. Introduction and Motivation

Wearable intelligent devices are nowadays an exciting new frontier and have become widely used in daily life. They are rendering the coming era of the Internet of Things (IoT); especially, smartwatches, after the success of smartphones, have attracted a lot of attention from industries and audiences [1]. Today, smartwatches and smart wristbands are experiencing a speedy development with strong demand in the mobile component market. However, they lack a multitechnology network connectivity [2]. Most of the smartwatches, due to their small size, contain antenna operating only in the ISM Band (Bluetooth and Wi-Fi) [3].

Significant progress is noticed in research regarding smartwatches and wearable devices antennas. An excellent comparison between microstrip patch, helical, and conical spiral antenna is developed in [4]. A multiband antenna operating in GSM900, LTE2300, and UMTS1900 is proposed in [5], the structure of the design sizes $55 \times 12 \times 4\ mm^3$ which make the antenna unsuitable for smartwatches. A miniaturized implantable ARRAY antenna was proposed in [6] and in [7], both array designs cover the GPS band entirely, but both of them do not cover the LTE bands and present big size. Wang et al. proposed a miniaturized antenna for GPS applications in [8], but the proposed antenna is difficult to manufacture and does not cover the UMTS or the LTE bands. Also, using a low-profile miniaturized antenna in [9], the authors present a good antenna that covers the LTE bands but the ISM band is not covered. In [10], a built-in antenna works perfectly in GPS and ISM bands, and the antenna is suitable for wearable devices such as smartwatch, but it is built with complex materials. In [11], Mehedi et al. designed a compact metamaterial-inspired antenna which operates at LTE and WiMAX frequency bands. Still, the ISM band is missing and the antenna presents a large size for smartwatch implementation. Zhao et al. proposed in [12] three cellular antenna designs for the smartwatch application by using the metal watch belt. The three designs cover the ISM, UMTS, and GSM bands entirely, but all of them are big-sized and complex for

implementing inside the smartwatch. In [14], Hasan et al. suggested a tri-band microwave perfect metamaterial absorber with miniature structure up to $10 \times 10 \times 1.6\,\text{mm}^3$; however, the design resonates at higher frequency bands 6.22 GHz, 8.76 GHz, and 13.05 GHz, which are not suitable for smartwatch application. Cheuk et al. designed in [15] a miniaturized printed inverted-F antenna for the Internet of Things, which sizes $15 \times 30\,\text{mm}^2$ but works only in the ISM and. An Electrically Compact SRR-Loaded Metamaterial Inspired Quad-Band Antenna for Bluetooth, Wi-Fi, WLAN, and WiMAX System is proposed in [16]; despite its complexity, the design is miniaturized sizing $30 \times 31\,\text{mm}^2$ and potentially suitable for wearable devices.

The objective of this research is to design a miniaturized integrated multiband antenna for smartwatches and wearable devices. The proposed antenna must operate in the following technologies UMTS1900, LTE2300, ISM2400, LTE2600, WIMAX5200, and ISM5800, satisfying the prerequisites in terms of gain, radiation pattern, current distribution, total efficiency, and reflection coefficient in each. Furthermore, the parametric study of the proposed antenna is discussed, and the influence of each parameter on the antenna performance in term of the reflection coefficient is presented. To ensure the compliance of the antenna against the FCC standards, the impact of design in terms of the SAR performance for the smartwatch application was evaluated. We used both the SAM head model provided by CST Studio and the human hand wrist model, designed based on the following layers: skin, fat, muscle, and bone. The SAR evaluation is calculated for the all selected frequencies and for different antenna positions: $d = 1\,\text{mm}$, $d = 2\,\text{mm}$, $d = 4\,\text{mm}$, and $d = 7\,\text{mm}$ for antenna on hand wrist configuration and $d = 1$, $d = 5\,\text{mm}$, and $d = 9\,\text{mm}$ for antenna next to SAM mouth configuration.

2. Requirements and Objective

2.1. Smartwatch Evolution and Hand Model. Smartwatches are now enjoying great success as the new technological trend in the mobile device market. Thanks to their ideal portability while inheriting the charm of classic watches, these devices are becoming more and more competitive by acquiring the features existing in smartphones. The criteria for the progression of smartwatches are reflected in their design, battery autonomy, and especially the development of applications compatible with the miniature display.

While internal hardware layers differ from a brand to another, most smartwatches have an electronic front display, either backlit LCD, OLED, or hologram [4]. Some use transflective or electronic paper, to consume less power. A rechargeable lithium-ion battery generally recharges them. Peripheral devices may include digital cameras, thermometers, accelerometers, pedometers, heart rate monitors, altimeters, barometers, compasses, GPS receivers, tiny speakers, and microSD cards, which are recognized as storage devices by many other kinds of computers. The software may include digital maps, schedulers and personal organizers, calculators, and various types of watch faces.

In smartwatches, efficient wireless performance is essential. Users expect these devices to last all day and stay connected all day. With the added challenges of implementing multiple antennas in an ultracompact form, it is absolutely essential to consider a multiband design to minimize space. This design should not contain any active component to reduce power consumption and should be miniaturized as much as possible to fit inside the device. As smartwatches can communicate with external devices such as sensors, wireless headsets, or machines, several wireless technologies may be required. In fact, a smartwatch can collect information from internal or external sensors and control or retrieve data from other instruments or servers via a local wireless network and then send it to an external server via the internet or long-range wireless network. For this reason, the proposed antenna should support the most popular wireless technologies such as UMTS1900, LTE2300, ISM2400, LTE2600, WIMAX5200, and ISM5800.

2.2. Antenna Requirement. The objective of this research is to design an integrated antenna having a planar structure and easy to manufacture, and such antenna is very suitable for smartwatch applications. The antenna should be miniature as possible and easy to deploy inside the smartwatch. The antenna must fit inside the smartwatch configuration as presented in Figure 1. The fact of implementing the antenna inside the smartwatch protects the antenna from vandalism, but it makes the wireless communication much difficult within a metal environment where the communication path is strongly influenced by the shielding of conductive layers. Since the smartwatch contains already conductive printed circuit boards (PCBs).

To ensure a general use case of the antenna, we selected the famous common bands in which our terminal should radiate. The target bands are listed in Table 1.

Regarding this frequency band specification, the antenna will ensure the IoT data acquisition through the IoT band and the data transmission through UMTS/LTE/WIMAX bands. The ISM bands can be used for local data transmission and to enable the IoT (communication with other devices). In each of the frequency bands listed in Table 1, the antenna must demonstrate compliance regarding its influence in terms of SAR on the wrist hand model presented in Figure 2 and the SAM head model.

3. Proposed Design

3.1. Configuration and Parametric Study. We started from an off-the-shelf planar antenna to obtain a low-cost design. We first design the UMTS/LTE2300/ISM band using the correlation between frequency and wavelength. Afterward, we create step by step the other bands also based on wavelength and taking into account that each new arm must not interfere in terms of the frequency band with the neighbor arm and must fit the sizing specifications of the antenna. In each designing step, we observe and study the current distribution in each frequency in order to adjust and optimize the structure. The configuration (a) refers to the coupling

between circuit (A) and the ground, giving the UMTS1900 and WIMAX5200 bands, whereas the configuration (a + b) refers to the coupling of circuits (A) and (B) ensuring the ISM2400 and LTE2600 bands and the enhancement of WIMAX5200 band. The configuration (a + b + c) is the coupling of circuits (A), (B), and (C) and the ground giving the band LTE2300 and providing additional enhancement to the other bands.

Figure 3 shows the four necessary steps of the conception of the design. Each step represents a target band, and in each stage, there was many simulations and iteration performed to obtain the best reflection coefficient. In Figure 4, we show the S_{11} result of each step and how the antenna resonates with each arm. The final results show additional frequencies obtained due to the mutual coupling between the components of the antenna.

3.2. Final Design. The feeding line sizes $2 \times 7\,mm^2$. The substrate made of FR4 material has a relative permittivity of 4.3 and a dielectric tangent loss up to 0.02, and it sizes $32 \times 35 \times 1.6\,mm^3$. The soldering spaces are modelled as PEC surfaces sizing $2 \times 4\,mm^2$. Table 2 summarizes the dimensions of the proposed antenna design and gives the value in mm of each parameter of the structure of the configuration shown in Figure 3.

4. Manufacturing and Measurement Results

In this section, the fabricated antenna is presented and obtained measurement results for the S_{11}, radiation pattern, gain, and current distribution are discussed.

4.1. Manufacturing. The proposed antenna model is fabricated using the LPKF ProtoLaser S systems which can process highly complicated tasks with printed circuit boards (PCBs). The machine is very efficient for cutting assembled PCBs, flexible PCBs, and cover layers. The manufactured antenna shown in Figure 5 was printed on an FR4 substrate, where the characteristics are listed in Table 2, and cut using the Maestro3 machine.

4.2. Measurement Setup. To measure the S_{11} of the antenna, the vector network analyzer (VNA) Agilent N3383 A 300 kHz–9 GHz is used, and it is calibrated in each simulation with the Agilent 85033E 3.5 mm calibration kit. The antenna was attached to the VNA through the Keysight 8121-0027 cable.

To perform the radiation pattern measurements, the double-ridged TEM horn antenna is used with Lens GZ0226DRH intended for indoor and outdoor ultra-wideband applications. The radiation measurement setup is described in Figure 6. The far-field antenna measurement system principle of operation is based on pulse measurement technique (time-domain measurements, TD). This system is applicable for most types of antennas and carries up sizes at distances R between antenna under test (AUT) and measuring antenna larger than far-field criteria [27]:

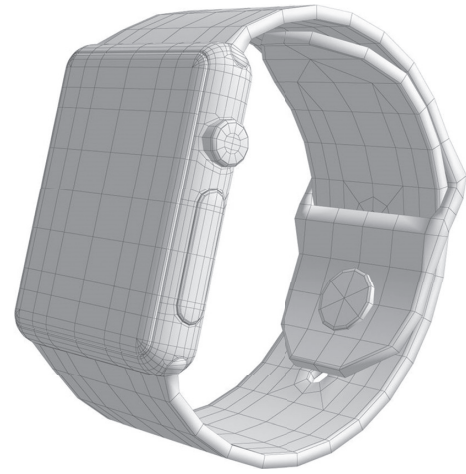

Figure 1: Smartwatch typical design.

Table 1: Frequency specification of the antenna design.

Frequency (GHz)	Bandwidth (MHz)	Designation
1.9	1920–2170	UMTS band
2.3	2305–2400	LTE2300 band
2.4	2400–2500	ISM band
2.6	2500–2690	LTE2600 band
5.2	5200–5300	WIMAX5200 band
5.8	5750–5850	ISM5800 band

$$R = \frac{2D^2}{\lambda}, \tag{1}$$

where D is the section (aperture) of antenna and λ is the wavelength. As main measurement instrument, the digital sampling converter is used. Its characteristics are optimized according to the system's parameters. The ultra-short-pulse electrical generator serves as measurement signal source.

The systems are built for frequency ranges 6 GHz, 12 GHz, 18 GHz, 26 GHz, and 40 GHz [27].

4.3. S_{11} Measurement Results. The simulation results compared to the measurement results in free space in terms of S_{11} with respect to 50 ohms are represented in Figure 7.

The measurement results confirm the results of simulation done with CST Studio software where all the target frequency bands fit the simulation resonance bands with small shift for the lowest frequencies up to 0.2 GHz. The first main reason is the line added in the manufactured design and one of the possible reasons explaining the larger bandwidth obtained in measurements is the multipath effect obtained by the environment where the measurements are performed and which is absent in the simulations. The results prove that the antenna meets perfectly the requirements in all the frequency bands discussed previously.

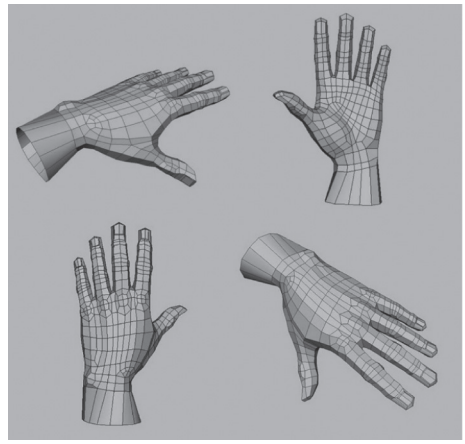

Figure 2: Hand model 3D design.

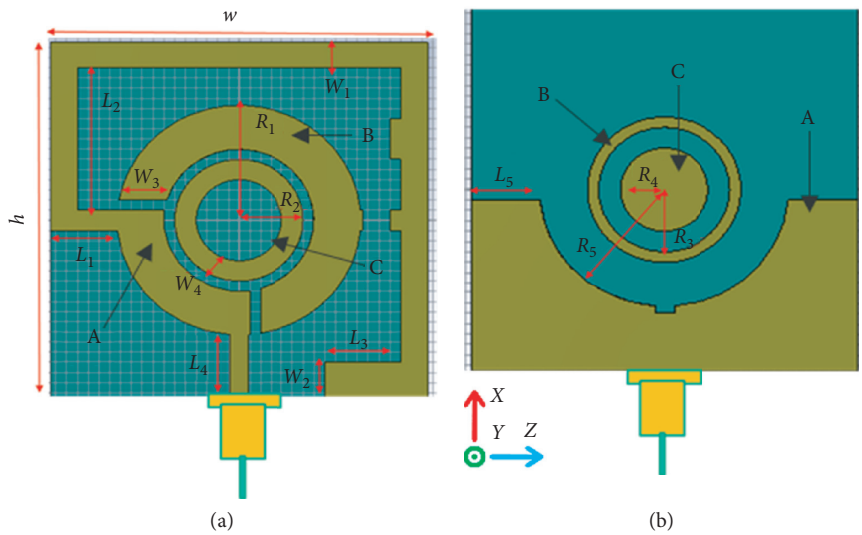

Figure 3: Antenna conception parameters: (a) top and (b) bottom. Each length is a parameter for the antenna conception.

4.4. Radiation Results. The radiation pattern of the gain in 2D plot (Phi = 0 and Phi = 90) is presented for each frequency at elevation view in Figure 8, and at azimuth view in Figure 9.

From the results plotted in Figures 8 and 9, it is observed that the antenna is approximately omnidirectional and it exhibits a higher gain for all the specified frequency bands. The best result in terms of radiation pattern shape is obtained for 2.3 GHz, for 2.4 GHz, and for 2.6 GHz where the antenna is clearly omnidirective and the corresponding maximum measured gains, respectively, are 3 dBi, 4.9 dBi, and 4.4 dBi. The antenna is more directive at 5.8 GHz with a maximum gain up to 6.6 dBi.

The Figure 10 shows the variation of the measured maximum gain in dBi in function of the frequency. It is noticeable that the minimum gain is 2 dBi obtained at 1.9 GHz and the maximum gain is 6.6 dBi at 5.8 GHz, and this means that the antenna has a high maximum gain over all the target frequency bands.

The total efficiency over frequency of the proposed design is presented in Figure 11. For the UMTS1900 and WIMAX5200 bands, the efficiency varies from 60% to 80%, but only around 60% for WIMAX5200 and LTE2300. The best results are obtained for ISM2400 and LTE2600 where the antenna total efficiency is 80%.

The Figure 12 represents the current distribution of the antenna in each frequency, showing which parts of the design interact to construct the target band.

4.5. Influence of the Smartwatch. After evaluating the reflection and the radiation measurements of the antenna in free space, the impact of the smartwatch on the performance of the antenna in terms of S_{11} is investigated. The radiation is not concerned since the smartwatch is a dielectric box with a relative permittivity of 2.3 and thus it does not prevent and or reflect the propagation of the antenna waves.

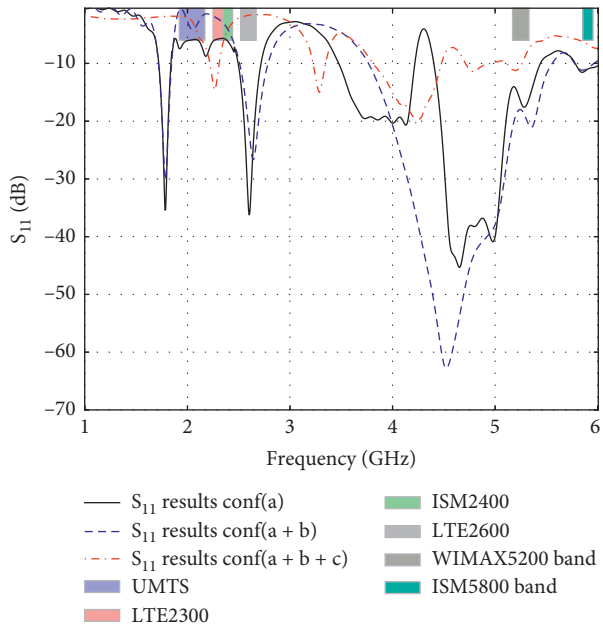

Figure 4: S_{11} simulation results of each configuration.

Figure 13 shows the influence of the smartwatch cover on the S_{11} parameter of the antenna. The S_{11} results of the antenna inside the smartwatch are compared to the S_{11} results of the antenna in free space. Four positions of the antenna were selected for this comparison: 0 mm (antenna attached to the cover of the smartwatch), 1 mm, and 2 mm separation of the antenna to the cover. As shown in Figure 13, it is noticeable that when the antenna is attached to the cover, the measured S_{11} of the antenna is increased dramatically. Starting from 1 mm as a separation, the S_{11} results get closed to the free space results. This explains why a gap between the antenna and the cover of the smartwatch is necessary.

5. Proposed Antenna Comparison to Existing Antenna

Table 3 shows the comparison between the proposed antenna and existing antennas based on size, coverage, bandwidth, gain, and applications.

6. SAR Studies

In this section, we evaluate the SAR performance of the antenna in two main scenarios: antenna mounted on the human hand wrist and antenna next to the human head mouth relevant for smartwatch with integrated microphone functionality. The SAR values are examined according to the standard limits defined by the FCC standards, which is 2 W/kg averaged over 10 g of tissue of the human head and 4 W/kg averaged over 10 g of tissue of the hand wrist [17, 19–26]. Figure 14(a) shows the position of the smartwatch antenna on the hand model with human hand tissues layers used for the SAR simulation with CST studio software, and Figure 14(b) shows the position of the smartwatch antenna next to the SAM head model provided by CST studio software.

Table 2: Dimensions of the proposed antenna.

Parameter	Value (mm)
h	32
w	35
L_1	6.6
L_2	21
L_3	4
L_4	27
L_5	16
W_1	26
W_2	21
W_3	4
Thickness	1.6
Gap	2
R_1	12
R_2	6
R_3	6
R_4	4
R_5	12

6.1. Antenna on the Hand Wrist. Figure 15 shows the setup of the antenna on the hand model. The antenna is placed in the center of the wrist at the top. To evaluate the SAR in each frequency, we choose four central values for the distance as separation between the antenna and the hand wrist: $d = 1$ mm, $d = 2$ mm, $d = 4$ mm, and $d = 7$ mm.

We designed a three-dimensional human hand model with four tissue layers: skin, fat, muscle, and bone. Table 4 summarizes the characteristics in terms of dielectric property and conductivity at each frequency for each tissue.

The SAR values averaged over a mass of 10 g of hand wrist tissue, for $d = 1$ mm, $d = 2$ mm, $d = 4$ mm, and

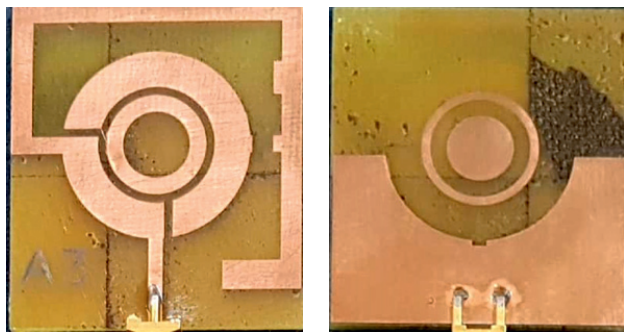

(a) (b)

Figure 5: Manufactured antenna design.

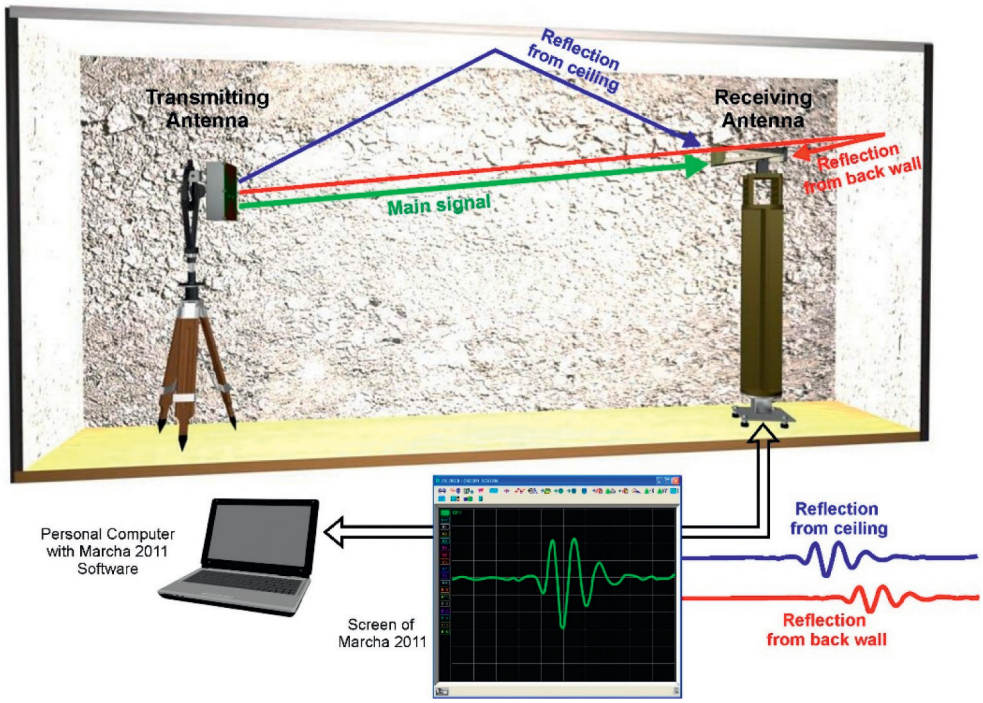

Figure 6: Measurement setup for the radiation pattern.

$d = 7$ mm, for each frequency and at each tissue layer, are summarized in Table 5. From the results obtained, it can be seen that the maximum SAR values in hand wrist case are below the limits 4 W/kg specified by the FCC standards. We notice that for all the frequencies in scope and at each distance, the SAR value calculated in fat tissue is in average 0.01 W/kg higher than the SAR value calculated in skin tissue. This can be explained by electrical properties ε_r and σ (S/m) of the fat tissue that are lower than the electrical properties of the skin tissue. In the other hand, the maximum SAR value decreases from the fat tissue to muscle tissue, and then from the muscle tissue to the bone tissue. We notice that the maximum SAR within the same tissue decreases as the frequency increases. In average, the maximum SAR decreases from 2.3 GHz to 5.8 GHz by 70% at the skin, fat, and muscle layers and by 45% at the bone layer.

Figure 16 shows the three-dimensional distributions of the SAR (W/kg) averaged over a mass of 10 g simulated inside the hand wrist model at the frequencies of 2.3 GHz, 2.4 GHz, 2.6 GHz and 3.500 GHz, 5.2 GHz, and 5.8 GHz with 5 mm spacing, using software CST MWS.

We notice that the averaged SAR over 10 g decreases slightly from the skin layer to the fat layer then decreases highly at the muscle layer to the bone. The values of the average SAR is higher in the center top of the wrist than the edges, which can be explained by the position of the antenna placed on the center of the hand wrist.

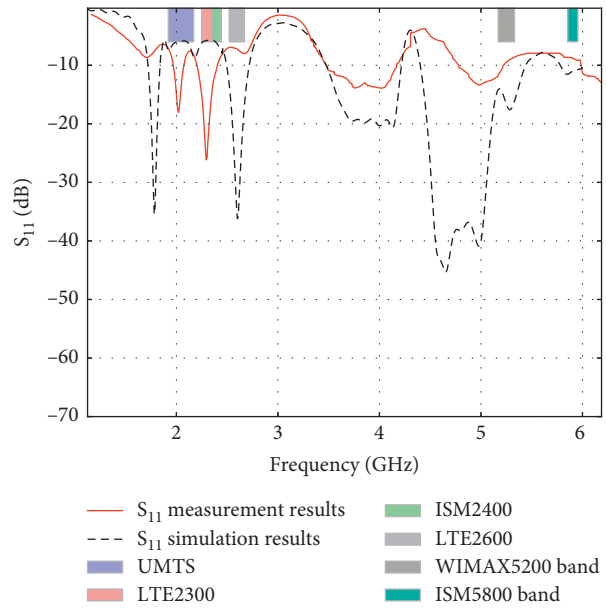

Figure 7: S_{11} simulation vs measurement results.

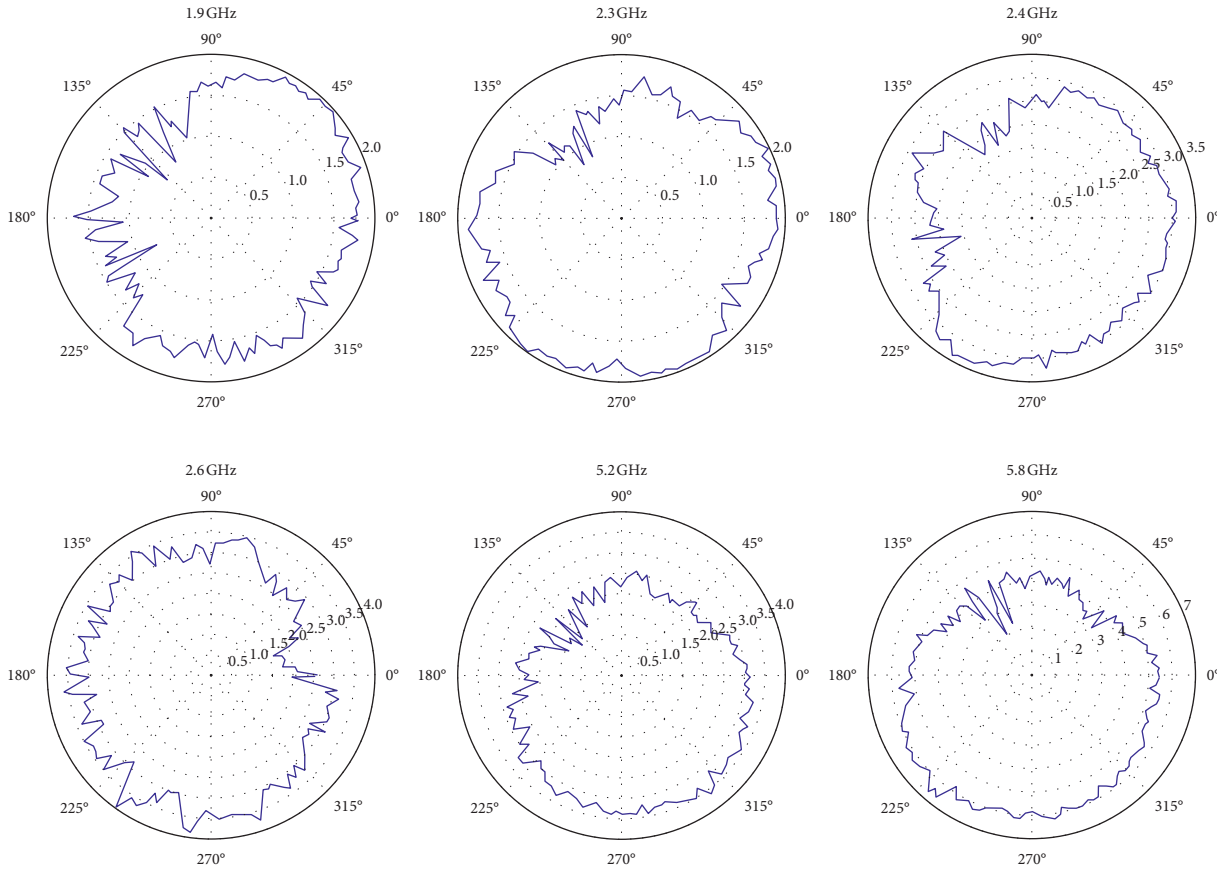

Figure 8: Elevation view of the radiation pattern.

Based on results obtained, we notice that all SAR values, at each hand wrist layer, fit the SAR requirements defined by the FCC standards 4 W/kg for the hand wrist.

6.2. Antenna next to SAM Mouth. In this configuration, the antenna is placed next to SAM mouth. We selected three values of the separation between the antenna and SAM

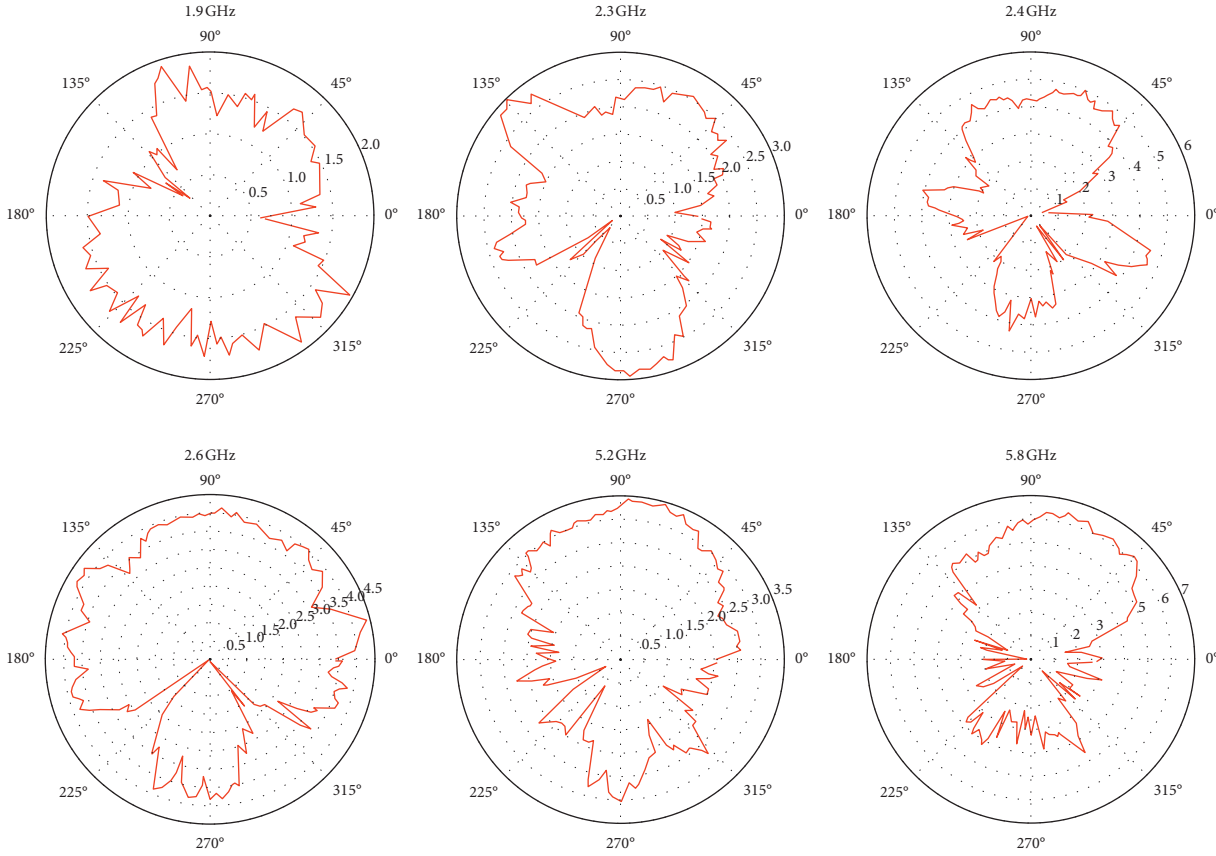

Figure 9: Azimuth view of the radiation pattern.

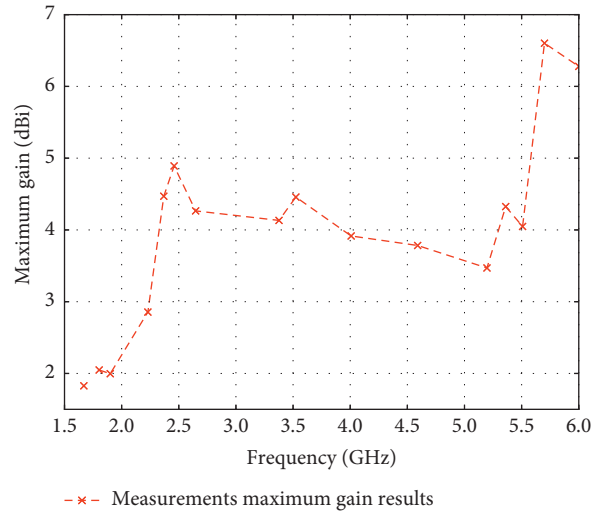

Figure 10: Variation of the maximum gain over frequencies.

mouth: $d = 1$ mm, $d = 5$ mm, and $d = 9$ mm. The simulated values of the maximum SAR averaged over a mass of 10 g of the tissues of the head for the SAM phantom head, at selected frequencies, using CST MWS software, are summarized in Table 6. From the results of electromagnetic simulations, we notice that the maximum SAR values for 10 g of the head model tissue decreases when the spacing between the antenna to SAM mouth changes from $d = 1$ mm to $d = 9$ mm. In average, the SAR value decreases by 60% from $d = 1$ mm to $d = 9$ mm. It is also noticeable that the SAR value is higher at higher frequencies 3500 MHz, 5200 MHz, and 5800 MHz.

We notice from the plots of SAR distribution inside SAM head that for the lowest frequencies 2300 MHz, 2400 MHz,

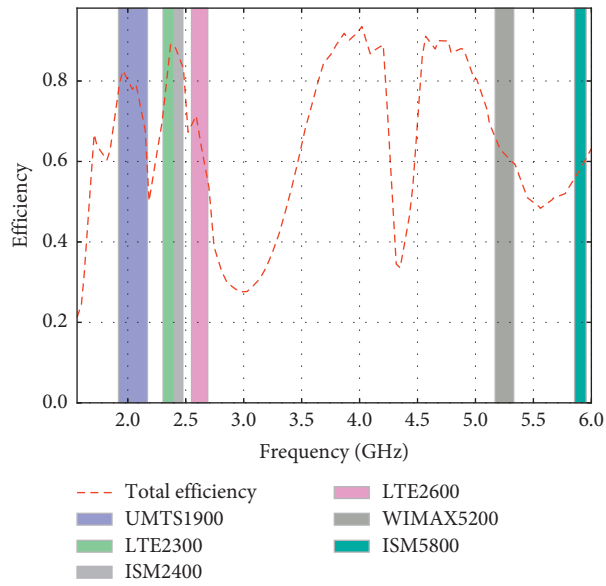

Figure 11: Variation of the total efficiency over frequencies.

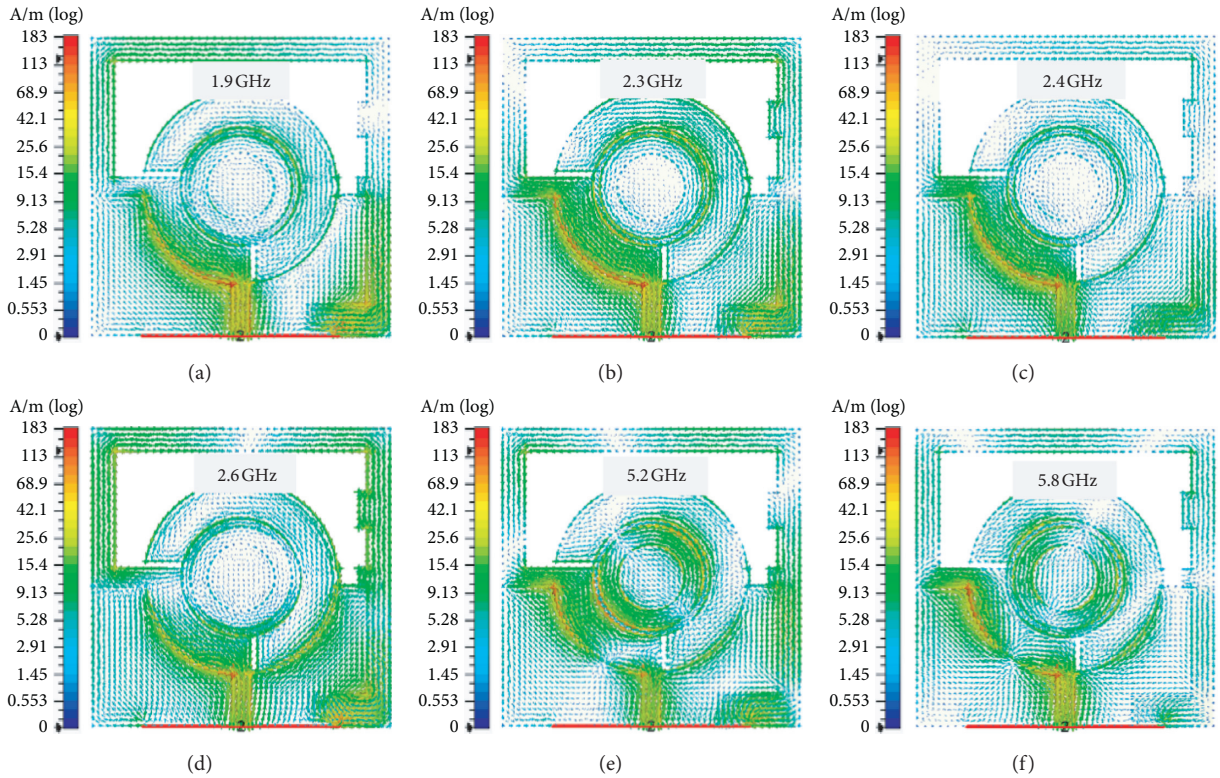

Figure 12: Current distribution of the antenna in each frequency.

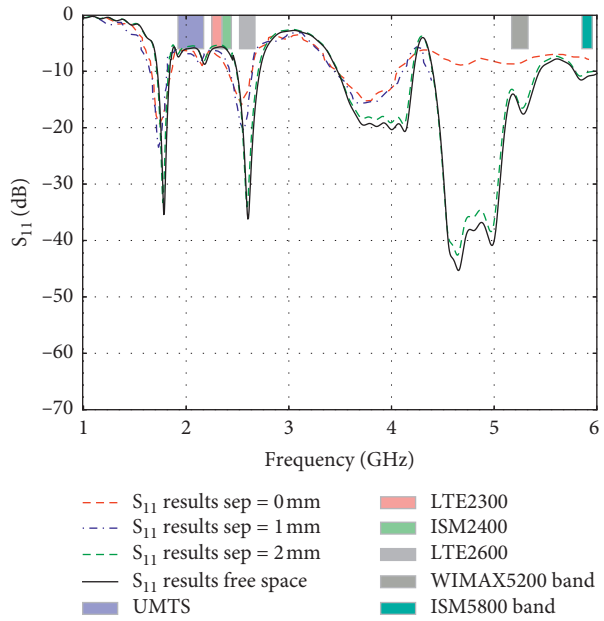

Figure 13: Influence of the smartwatch on the antenna S_{11}.

Table 3: Performance comparison between the proposed antennas with the existing antennas.

References	Antenna dimension (mm^2)	Resonant frequencies (GHz)	Maximum gain (dBi)	Applications
Zhao et al. [17]	40 × 124	0.7, 1.8	3.8	Bluetooth, WLAN, WiMAX
Wu et al. [18]	40 × 38	2.47, 5.18	7.0	WLAN
Chung et al. [10]	33 × 41	1.54, 2.41, 3.25	3.0	GPS, WLAN, WiMAX
Mehedi et al. [11]	42 × 33	0.63, 3.21, 3.63	3.69	LTE, WiMAX
Hasan et al. [16]	31 × 30	2.4, 3.5	2.25	ISM2400, WIMAX3500
Cheuk et al. [15]	30 × 15	2.4	4	ISM2400
Proposed antenna	35 × 32	1.9, 2.3, 2.4, 2.6, 5.2, 5.8	6.6	UMTS, LTE2300, ISM2400, LTE2600, WIMAX5200, ISM5800

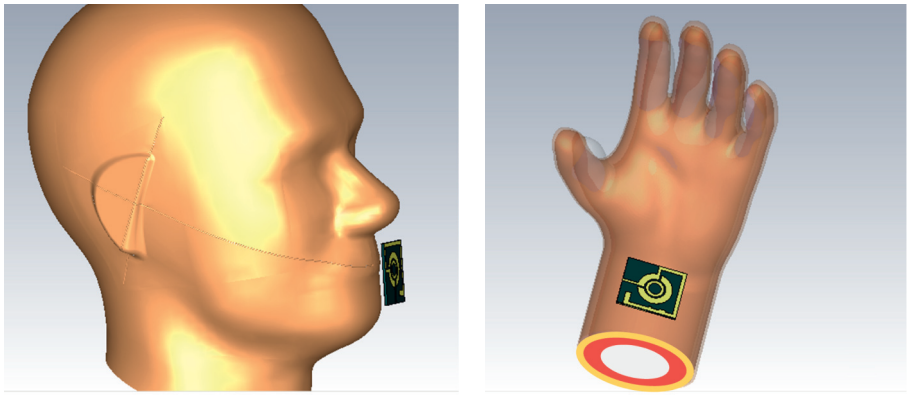

(a) (b)

Figure 14: Position of smartwatch antenna: (a) next to SAM mouth model; (b) on the hand wrist model with 4 tissues.

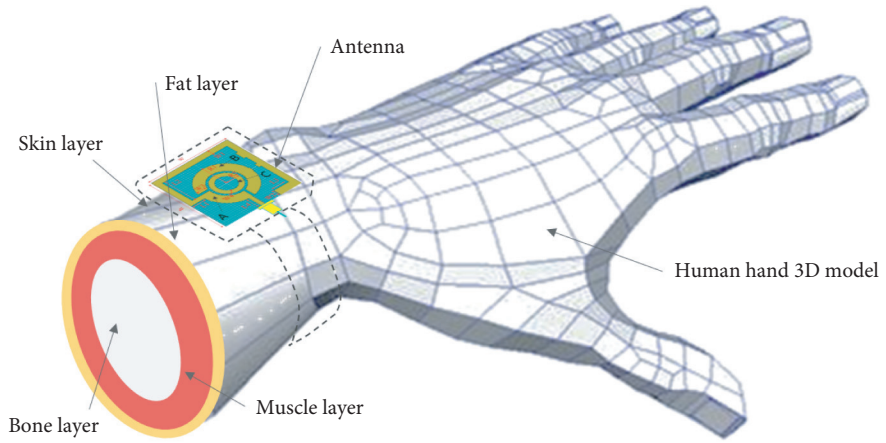

Figure 15: SAR simulation setup.

Table 4: Human hand tissue characteristics [19].

Frequency (MHz)	2400		2600		5200		5800	
Tissues	ε_r	σ (S/m)	ε_r	σ (S/m)	ε_r	σ (S/m)	ε_r	σ (S/m)
Skin	43.8	0.86	38.43	1.30	38.18	1.40	38.06	1.44
Fat	11.3	0.11	5.32	0.09	5.30	0.10	5.28	0.10
Muscle	55.9	0.97	54.04	1.57	53.77	1.70	53.64	1.77
Bone	20.8	0.34	15.28	0.50	15.10	0.56	15.01	0.59

Table 5: SAR result table of antenna mounted on the hand.

	Distance		$d = 1$ mm	$d = 2$ mm	$d = 4$ mm	$d = 7$ mm
Frequency (MHz)	Tissue	Input power (W)	10 g SAR (W/kg)	10 g SAR (W/kg)	10 g SAR (W/kg)	10 g SAR (W/kg)
2300	Skin	0.125	2.29	0.73	0.69	0.36
	Fat	0.125	2.30	0.74	0.70	0.37
	Muscle	0.125	1.25	0.65	0.61	0.21
	Bone	0.125	0.44	0.27	0.24	0.14
2400	Skin	0.125	2.31	0.68	0.62	0.48
	Fat	0.125	2.32	0.69	0.63	0.49
	Muscle	0.125	1.30	0.58	0.51	0.44
	Bone	0.125	0.32	0.24	0.21	0.15
2600	Skin	0.125	2.61	0.90	0.68	0.42
	Fat	0.125	2.62	0.91	0.69	0.43
	Muscle	0.125	2.10	0.83	0.54	0.41
	Bone	0.125	0.36	0.29	0.25	0.14
3500	Skin	0.125	3.31	2.18	1.98	1.49
	Fat	0.125	3.32	2.19	1.99	1.50
	Muscle	0.125	2.17	2.05	1.53	1.32
	Bone	0.125	0.58	0.56	0.50	0.40
5200	Skin	0.125	3.66	3.72	2.79	1.86
	Fat	0.125	3.67	3.73	2.80	1.87
	Muscle	0.125	2.88	3.39	2.35	1.6
	Bone	0.125	0.40	0.51	2.16	0.30
5800	Skin	0.125	3.50	3.37	2.17	0.86
	Fat	0.125	3.51	3.38	1.68	0.87
	Muscle	0.125	2.82	2.91	1.53	0.77
	Bone	0.125	0.27	0.35	0.27	0.17

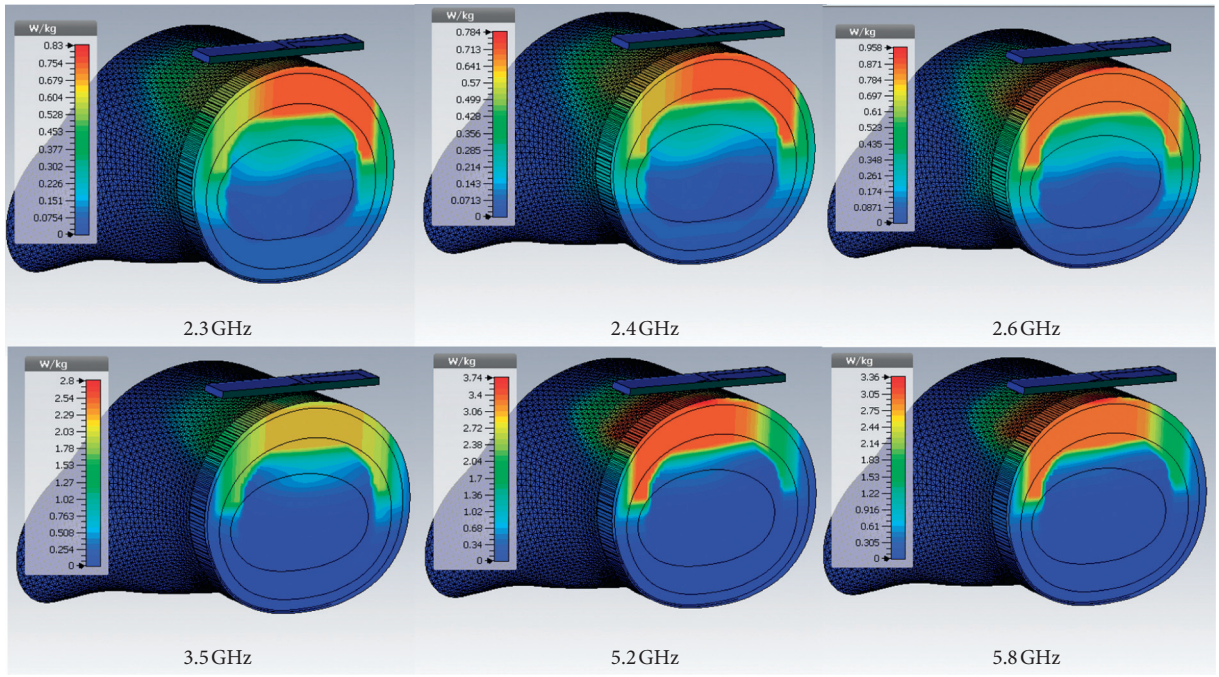

Figure 16: SAR (W/kg) distribution averaged over 10 g inside the hand wrist, for a spacing $d = 2$ mm.

Table 6: Maximum SAR results at each frequency for each distance of antenna next to mouth.

Frequency (MHz)	Distance Tissue	Input power (W)	$d = 1$ mm 10 g SAR (W/kg)	$d = 5$ mm 10 g SAR (W/kg)	$d = 9$ mm 10 g SAR (W/kg)
2300	SAM head	0.125	0.60	0.49	0.35
2400	SAM head	0.125	0.78	0.40	0.27
2600	SAM head	0.125	0.76	0.37	0.23
3500	SAM head	0.125	1.98	1.19	0.88
5200	SAM head	0.125	1.79	1.20	0.64
5800	SAM head	0.125	1.90	0.96	0.55

and 2600 MHz, the SAR values are higher with more considerable surface impact deep inside SAM head. However, for the highest frequencies 3500 MHz, 5200 MHz, and 5800 MHz, the SAR values are lower with smaller surface impact deep inside SAM head.

Based on the results shown in Table 6 and Figure 17, all the values of the SAR averaged over 10 g inside SAM head obtained at each frequency starting from a separation of 1 mm are below the SAR limits 2 W/kg defined by the FCC standards.

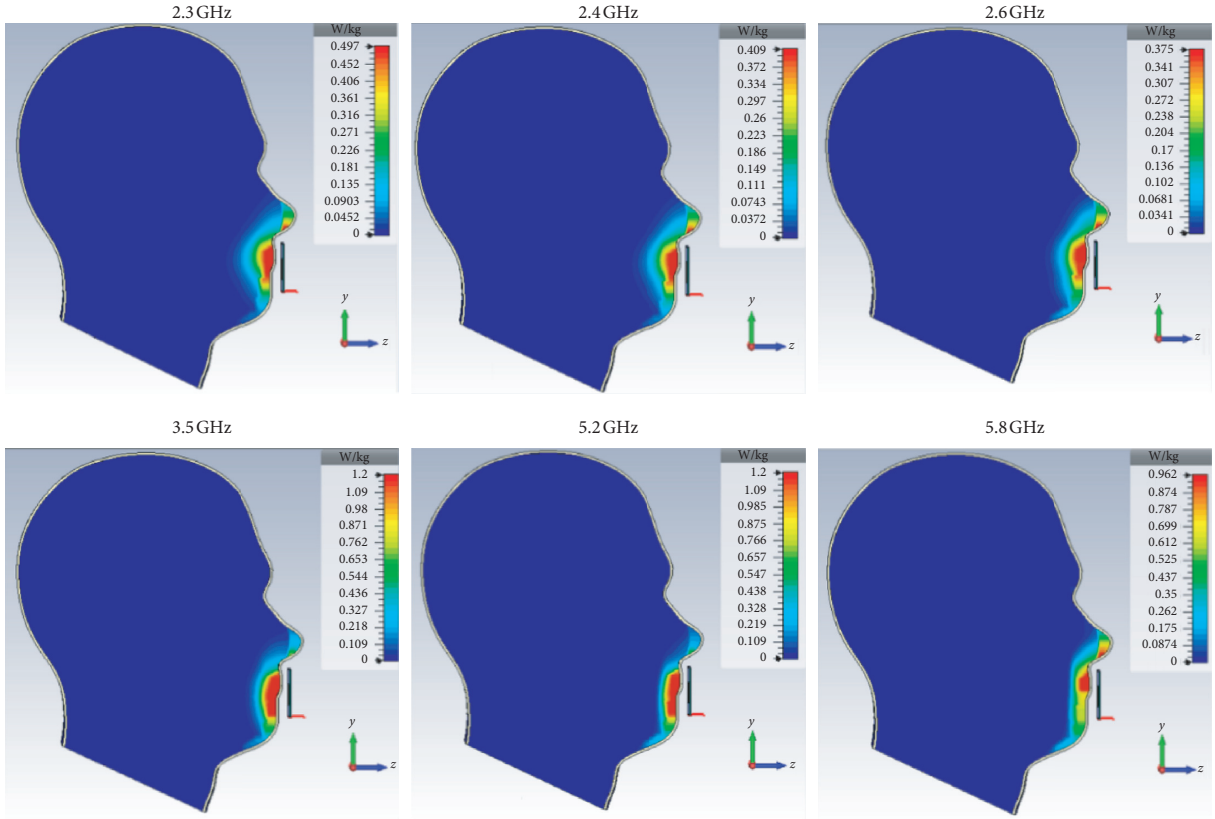

Figure 17: SAR (W/kg) distribution averaged over 10 g inside SAM head, antenna 5 mm separated to SAM mouth.

7. Conclusions

In this paper, a novel miniaturized antenna experimentally verified for wearable device applications is presented. The antenna with its simple low-cost planar structure allows manufacturer to save considerable amount of money accounting of the number of antennas required in such application in the worldwide. Comparatively, to the existing propositions, the presented antenna sizing $32 \times 35 \times 1.6\ \text{mm}^3$ is distinguished by its simplicity for manufacturing, ease of deployment inside smartwatches, and excellent performance in terms of radiation pattern, total efficiency, gain, and reflection coefficient. The antenna was fabricated and measured in terms of the radiation pattern and the reflection coefficient, the results confirm the simulations and show that the antenna is approximately omnidirectional with a maximum gain up to 6.6 dBi and S_{11} up to −22 dB, and it covers all the specified technology bands used in the smartwatch devices such as UMTS1900, LTE2300, ISM2400, LTE2600, WIMAX5200, and ISM5800. For the compliance of antenna against the FCC standards, the SAR averaged for 10 g of tissue was evaluated for each frequency and for two configurations: antenna on the hand wrist model with four tissue layers and antenna next to the SAM mouth model. The maximum SAR results obtained starting from a separation of 1 mm shows compliant values below the limit 4 W/kg in the case of the hand wrist and values below 2 W/kg limit in case of SAM head.

Data Availability

The data used to support the findings of this study are available from the corresponding author upon request.

Conflicts of Interest

The authors declare that they have no conflicts of interest.

Acknowledgments

The authors would like to express their great appreciation to Professor Angel Mediavilla from the University of Cantabria for his kind support and assistance and Professor Mohammed Harrag for his help and advice.

References

[1] R. Brunet-Thornton and F. Martinez, *Analyzing the Impacts of Industry 4.0 in Modern Business Environments*, IGI Global, Hershey, PA, USA, 2018.

[2] A. Jayaram, "Lean six sigma approach for global supply chain management using industry 4.0 and IIoT," in *Proceedings of the 2016 2nd International Conference on Contemporary Computing and Informatics (IC3I)*, pp. 89–94, Noida, India, 2016.

[3] F. Bonavolont, A. Tedesco, R. S. L. Moriello, and A. Tufano, "Enabling wireless technologies for industry 4.0: State of the art," in *Proceedings of the IEEE International Workshop on*

Measurement and Networking (MN), pp. 1–5, Naples, Italy, 2017.

[4] R. Kazemi, J. Palmer, F. Quaiyum, and A. E. Fathy, "Steerable miniaturized printed quadrifilar helical array antenna using digital phase shifters for BGAN/GPS applications," *IET Microwaves, Antennas and Propagation*, vol. 12, no. 7, pp. 1196–1204, 2018.

[5] Y. Hong, J. Tak, J. Baek, M. Bongsik, and J. Choi, "Design of a multiband antenna for LTE/GSM/UMTS band operation," *International Journal of Antennas and Propagation*, vol. 2014, p. 9, Article ID 548160, 2014.

[6] P. Zhou, M. He, Y. Hao, C. Zhang, and Z. Zhang, "Design of a small-size broadband circularly polarized microstrip antenna array," *International Journal of Antennas and Propagation*, vol. 2018, p. 12, Article ID 5691561, 2018.

[7] A. Vasylchenko, Y. Schols, W. De Raedt, and G. A. E. Vandenbosch, "Quality assessment of computational techniques and software tools for planar antenna analysis," *IEEE Antennas Propagat. Magazine*, vol. 51, no. 1, pp. 23–38, 2009.

[8] R. Senathong, S. Niyamanon, and C. Phongcharoenpanich, "Dual-frequency circularly-polarized truncated square aperture patch antenna with slant strip and L-shaped slot for WLAN applications," *International Journal of Antennas and Propagation*, vol. 2018, Article ID 7684742, 2018.

[9] H. Liu, B. Lu, and L. Li, "Novel miniaturized octaband Antenna for LTE smart handset applications," *International Journal of Antennas and Propagation*, vol. 2015, p. 8, Article ID 861016, 2015.

[10] M. A. Chung and C. F. Yang, "Built-in antenna design for 2.4 GHz ISM band and GPS operations in a wrist-worn wireless communication device," *IET Microwaves, Antennas Propagation*, vol. 10, no. 12, pp. 1285–1291, 2016.

[11] M. M. Hasan, M. R. I. Faruque, M. R. I. Faruque, and M. T. Islam, "Dual band metamaterial antenna for LTE/Bluetooth/WiMAX system," *Scientific Reports*, vol. 8, no. 1, p. 1240, 2018.

[12] D. Wen, Y. Hao, H. Wang, and H. Zhou, "Design of a MIMO antenna with high isolation for smartwatch applications using the theory of characteristic modes," *IEEE Transactions on Antennas and Propagation*, vol. 67, no. 3, pp. 1437–1447, 2019.

[13] Y. Li and W. Yu, "A miniaturized triple band monopole antenna for WLAN and WiMAX applications," *International Journal of Antennas and Propagation*, vol. 2015, p. 5, Article ID 146780, 2015.

[14] M. M. Hasan, M. R. I. Faruque, and M. T. Islam, "A tri-band microwave perfect metamaterial absorber," *Microwave and Optical Technology Letters*, vol. 59, no. 9, pp. 2302–2307, 2017.

[15] C. Yin Cheung, J. S. M. Yuen, and S. W. Y. Mung, "Miniaturized printed inverted-F antenna for internet of things: a design on PCB with a meandering line and shorting strip," *International Journal of Antennas and Propagation*, vol. 2018, p. 5, Article ID 5172960, 2018.

[16] M. Hasan, M. Rahman, M. R. I. Faruque, M. T. Islam, and M. U. Khandaker, "Electrically compact SRR-loaded metamaterial inspired quad band antenna for bluetooth/WiFi/WLAN/WiMAX system," *Electronics*, vol. 8, no. 7, p. 790, 2019.

[17] K. Zhao, Z. Ying, and S. He, "Antenna designs of smart watch for cellular communications by using metal belt," in *Proceedings of 9th European Conference on Antennas and Propagation (EuCAP)*, Lisbon, Portugal, 2015.

[18] Di Wu, S. W. Cheung, Q. L. Li, and T. I. Yuk, "Slot antenna for all-metal Smartwatch applications," in *Proceedings of 10th European Conference on Antennas and Propagation (EuCAP)*, Davos, Switzerland, 2016.

[19] 2020 http://transition.fcc.gov/oet/rfsafety/dielectric.html.

[20] Federal Communications Commission, *Specifc Absorption Rate (SAR) for Cellular Telephones*, Federal Communications Commission, Washington, DC, USA, 2012, https://www.fcc.gov/general/cell-phones-and-specific-absorption-rate.

[21] Federal Communications Commission, *Evaluating Compliance with FCC Guidelines for Human Exposure to Radiofrequency Electromagnetic Fields*, Federal Communications Commission, Washington, DC, USA, 2001.

[22] International commission on non-ionizing radiation protection, "ICNIRP guidelines: for limiting exposure to time-varying electric, magnetic and electromagnetic fields (up to 300 GHz)," *Health Physics*, vol. 99, no. 6, 2010.

[23] Federal Communications Commission, *Wireless-Devices-and-Health-Concerns*, Washington, DC, USA, 2018, https://www.fcc.gov/consumers/guides/wireless-devices-and-health-concerns.

[24] T. Wu, T. Rappaport, and C. Collins, "The human body and millimeter-wave wireless communication systems: interactions and implications," in *Proceedings of IEEE International Conference on Communications (ICC)*, London, UK, June 2015.

[25] Federal Communications Commission, *SAR-Test-Report-4197534*, Federal Communications Commission, Washington, DC, USA, 2019, https://fccid.io/2AHZ7100602018/RF-Exposure-Info/SAR-Test-Report-4197534.

[26] H. M. Madjar, "Human radio frequency exposure limits: an update of reference levels in Europe, USA, Canada, China, Japan and Korea," in *Proceedings of the 2006 IEEE International Symposium on Electromagnetic Compatibility, EMC EUROPE*, Wroclaw, Poland, September 2016.

[27] B. Fady, J. Terhzaz, A. Tribak, F. Riouch, and A. Mediavilla, "Novel miniaturized multiband antenna and applications for smart navigation media," *International Journal of RF and Microwave Computer-Aided Engineering*, vol. 29, Article ID e21940, 2019.